Supplemental Material to "Valley-tunable, even-denominator fractional quantum Hall state in the lowest Landau level of an anisotropic system"

Md. Shafayat Hossain,[1] Meng K. Ma,[1] Y. J. Chung,[1] S. K. Singh,[1] A. Gupta,[1] K. W. West,[1] K. W. Baldwin,[1] L. N. Pfeiffer,[1] R. Winkler,[2] and M. Shayegan[1]

[1]*Department of Electrical and Computer Engineering, Princeton University, Princeton, New Jersey 08544, USA*

[2]*Department of Physics, Northern Illinois University, DeKalb, Illinois 60115, USA*

(Dated: March 20, 2023)

I. MATERIALS AND METHODS

Our sample is grown via molecular beam epitaxy on a GaAs substrate. It contains a 45-nm-wide AlAs quantum well (QW), sandwiched by 150-nm-thick $Al_{0.33}Ga_{0.67}$ barriers, and modulation doped with Si δ-layers (Fig. S1). Similar to the case of GaAs, as long as the conduction band offset between the barrier and the QW is sufficiently large, it is possible to confine carriers in the AlAs QW through modulation doping [1–4]. The main difference is that in AlAs the conduction band has lower energy at the X points of the Brillouin zone instead of the Γ point. Therefore, the electrons in our AlAs QW are confined in the X-point valleys. Our AlAs QW has a density of $\simeq 1.45\times10^{11}$ cm^{-2} with a low-temperature mobility of 7.5×10^5 cm^2/Vs. Details of the growth of such very high-quality AlAs two-dimensional electron system (2DES) can be found in Ref. [4].

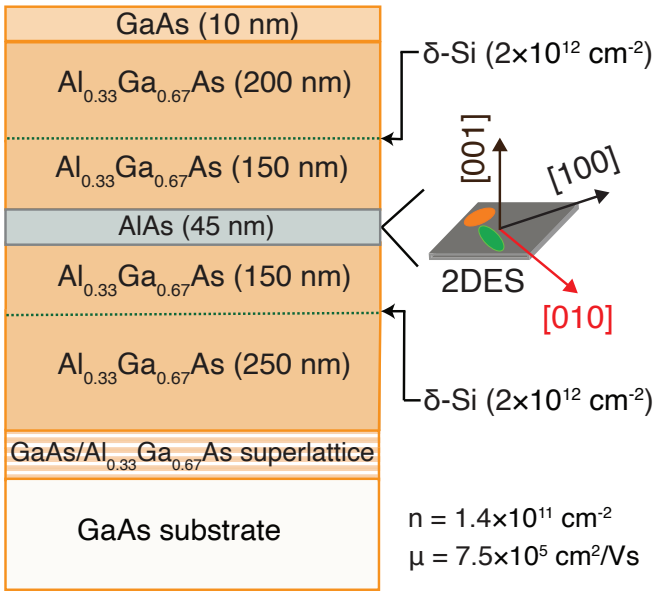


FIG. S1. Structure of our AlAs 2DES grown on a GaAs substrate. The growth direction is [001]. The AlAs layer is under compressive biaxial strain because of the slightly larger lattice constant of AlAs relative to GaAs. This strain results in the occupancy of X and Y valleys only.

In bulk AlAs, electrons occupy three energetically-degenerate ellipsoidal (or six half-ellipsoidal) conduction-band valleys at the six equivalent X points of the first Brillouin zone [3]; see Fig. S2(a). We denote these valleys as X, Y, and Z with their major axes lying along [100], [010], and [001], respectively [see Fig. S2(a)]. The electrons in each valley possess an anisotropic Fermi surface with longitudinal and transverse effective masses of $m_l = 1.1$ and $m_t = 0.20$, in units of the free electron mass.

When an AlAs QW is formed along the [001] axis, the confinement in the growth direction splits the three-fold valley degeneracy because of the difference in the effective mass along the in-plane and out-of-plane directions. We refer to the out-of-plane valley as Z and the in-plane valleys as X and Y. At first sight, one would expect that the Z valley should be occupied at all well widths since it has the larger effective mass along the confinement direction. However, the slightly larger lattice constant of AlAs compared to GaAs causes biaxial compression in the plane of the AlAs layer, lowering the conduction band of the X and Y valleys relative to the Z valley. This causes the ground-state energies of the two types of valleys to cross at a critical QW width of $\simeq 6$ nm [3]. Above this well-width, the X and Y valleys are occupied; this is the case for our 45-nm-wide AlAs QW [Figs. S1 and S2(b)].

In the absence of any additional in-plane strain, electrons in our AlAs QW occupy two in-plane valleys (X and Y). This two-fold valley degeneracy can be lifted via the application of an in-plane, symmetry-breaking, strain $\varepsilon = \varepsilon_{[100]} - \varepsilon_{[010]}$, where $\varepsilon_{[100]}$ and $\varepsilon_{[010]}$ are the strain values along [100] and [010] [3]. The valley splitting energy is given by $E_V = \varepsilon E_2$, where E_2 is the deformation potential, which in AlAs has a band value of 5.8 eV. Positive strain pushes the energy of the X valley up relative to the Y valley, causing electrons to transfer from X to Y, and vice versa for negative strain.

In Fig. S2(c) we show our experimental setup for applying tunable in-plane strain to the 2DES. We glue the sample on one side of a stacked piezoelectric lead-zirconate-titanate (PZT) actuator with a commercial two-part epoxy [5]. The piezoelectric actuator deforms when a voltage (V_P) is applied across its two leads and hence strains the sample glued to its side. Thus, we introduce nearly uniaxial, in-plane strain to our 2DES.

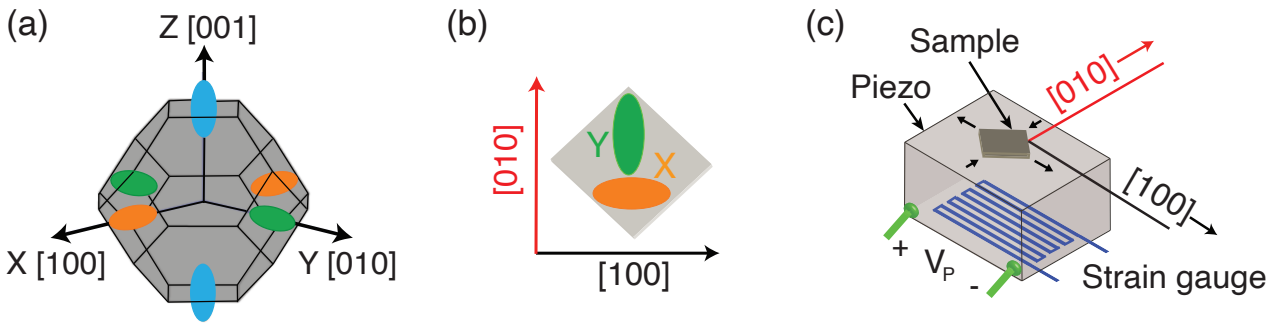


FIG. S2. (a) First Brillouin zone and constant energy surfaces of the lowest energy bands for bulk AlAs, showing the X, Y, and Z valleys; [100], [010], and [001] refer to the crystallographic directions. (b) The sample geometry, including the orientation of the two occupied valleys (X and Y) and the directions along which the longitudinal resistances ($R_{[100]}$ and $R_{[010]}$) are measured are shown. (c) Schematic of the experimental setup for applying in-plane strain (ε). The sample and a strain gauge are glued to the opposite sides of a piezo-actuator, and strain is introduced when a bias voltage (V_P) is applied to the actuator's leads.

The amount of strain can be measured by a strain gauge glued on the back-side of the piezo-electric actuator [Fig. S2(c)]. We find the strain to be 3.3×10^{-7} per Volt applied to the piezo-actuator.

In order to maintain sufficient strain homogeneity, we used very small van der Pauw samples with dimensions of 1.5 mm ×1.5 mm. Note that the sample edges are along the GaAs cleave directions, [110] and [$\bar{1}$10] [see Fig. S2(b)]. The samples are lapped and polished on the backside down to $\simeq 150$ μm in order for the strain to propagate to the 2DES [5]. Electron-beam-evaporated Ti-Au alloy on the backside of the sample shields the 2DES from the electric field generated by the applied V_P.

We note that during the cooldown, because of the difference in the thermal contraction coefficients of the sample and piezo, a residual strain [strain at $V_P = 0$ in Fig. 2(d)] develops. We can compensate for this residual strain by applying a uniaxial strain with opposite sign via the piezo actuator to attain the $\varepsilon = 0$ condition [3, 5].

In Fig. S3 we show the voltage and current leads for all the configurations used in our magnetotransport measurements. We carried out our experiments mostly in a dilution refrigerator with a mixing chamber temperature of $T \simeq 0.03$ K and using an 18 T superconducting magnet at the National High Magnetic Field Laboratory (NHMFL) in Tallahassee, Florida.

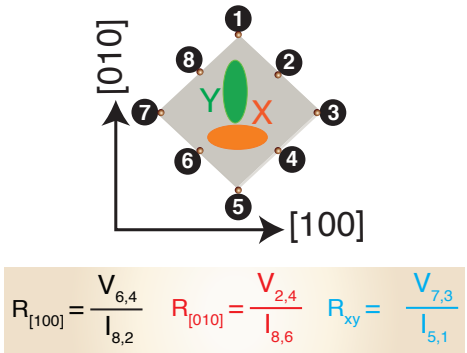


FIG. S3. Configurations showing the current injection and voltage probes used to measure $R_{[100]}$, $R_{[010]}$, and R_{xy}.

II. TEMPERATURE DEPENDENCE OF THE $\nu = 1/2$ FQHS

In Figs. 4 (c, d) of the main text, we showed the extraction of an activation gap at $\nu = 1/2$. Here we show the temperature-dependent magnetoresistance data near the 1/2 fractional quantum Hall state (FQHS) when only the X valley is occupied [Fig. S4(a)], and when only the Y valley is occupied [Fig. S4(a)].

III. TILT EVOLUTION OF $\nu = 1/2$ FOR BI-VALLEY 2DES

Here we show the tilt evolution data at $\varepsilon \simeq 0$ when electrons occupy the X and Y valleys equally at $B_{||} = 0$. Figure S5 shows such data. Similar to the cases where only X or Y valley are occupied (Fig. 3 of the main text), we observe a qualitatively similar tilt evolution at $\nu = 1/2$: from a compressible phase to an incompressible FQHS and eventually to an insulating phase as the tilt angle (θ) is increased. Intriguingly, as stated in the main text, the values of θ where the phase transitions occur fall very close to the case where only the Y valley is occupied. This can be understood from the $B_{||}$-induced valley imbalance as discussed by Gokmen *et al.* [6]. The direction of $B_{||}$ in our experiments is always along [100]. According to Gokmen *et al.* [6] and our discussion in the main text, this should cause a transfer of electrons from the X valley to the Y valley.

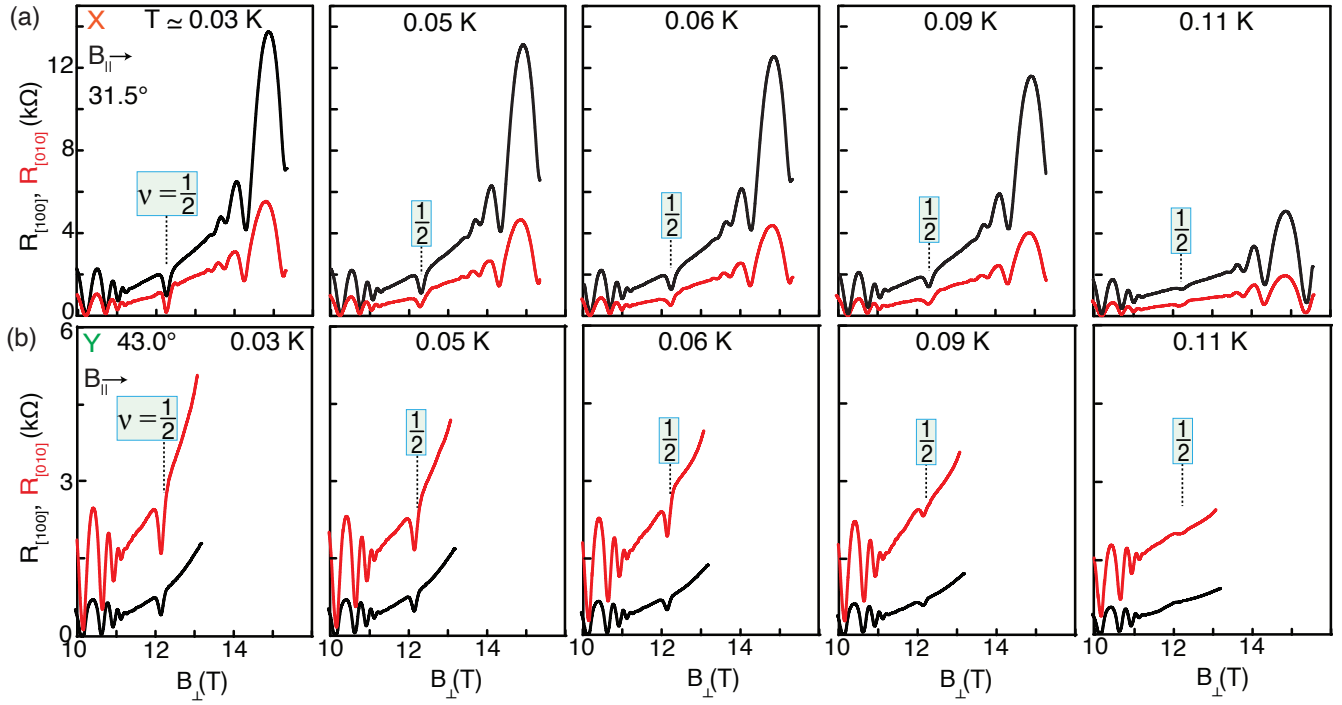


FIG. S4. Temperature dependence of the magnetoresistance in the extreme quantum limit when the 2D electrons occupy only (a) X valley at $\theta = 31.5^o$ and (b) Y valley at $\theta = 43^o$. Plotted are $R_{[100]}$ (black) and $R_{[010]}$ (red) for five different T ranging from $\simeq 0.03$ to 0.11 K.

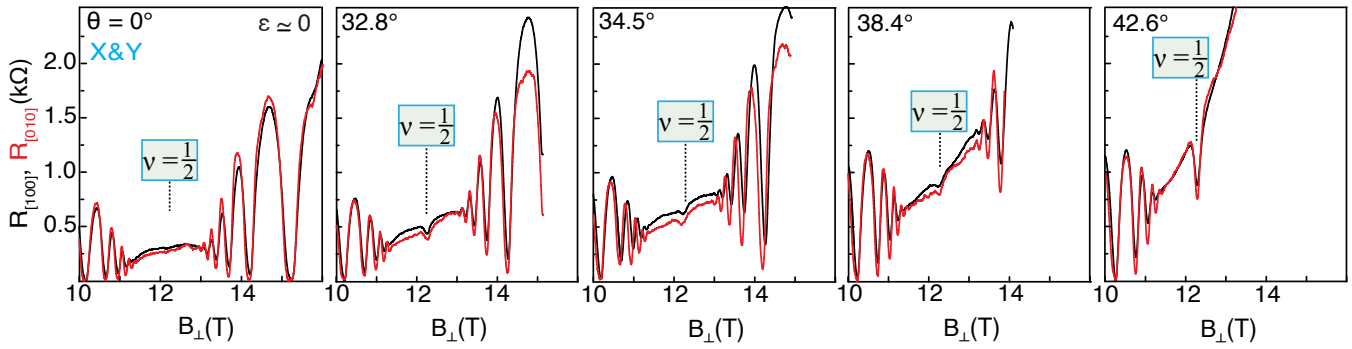


FIG. S5. Tilt-evolution of the magnetoresistance data near $\nu = 1/2$ when $\varepsilon \simeq 0$, taken at $T \simeq 0.03$ K. The direction of $B_{||}$ is along [100], i.e., along $R_{[100]}$. Similar to the single-valley cases, $\nu = 1/2$ undergoes phase transitions from a compressible phase to an incompressible FQHS, and then finally to an insulating phase as we increase θ.

IV. EVOLUTION OF ELECTRON CHARGE DISTRIBUTION AND FERMI SEA WITH $B_{||}$

In this section we elaborate on the impact of $B_{||}$ on the charge distribution and Fermi seas of electrons at $B_\perp = 0$. To facilitate the discussion, in Fig. S6, we re-show Fig. 3 of the main text and include electron Fermi seas at $B_\perp = 0$ calculated for $B_{||}$ values (applied along [100]) experienced by electrons at $\nu = 1/2$.

As discussed in the main text, the differences in $B_{||}$ values required to observe a strong FQHS at $\nu = 1/2$ possibly stems from the influence of $B_{||}$ on the charge distribution and interlayer tunneling. In a quasi-2DES with finite electron layer thickness, the impact of $B_{||}$ depends on the electron's orbital motion and its effective mass in the direction perpendicular to $B_{||}$ [7]. Our calculated charge distributions, shown as insets in Fig. S6 plots, become more bilayer like at a much smaller θ in (a) compared to (b). This is consistent with the appearance of the $\nu = 1/2$ FQHS at smaller θ in (a), assuming that an appropriate (intermediate) amount of tunneling is required to observe the 1/2 FQHS [8–10]. To clarify this, in Fig. S7 we show the calculated charge distributions for X [Fig. S7(a)] and Y [Fig. S7(b)] valley electrons for different $B_{||}$ values, applied along [100]. As seen in Fig. S7, the charge distributions at $B_{||} = 0$ for the two

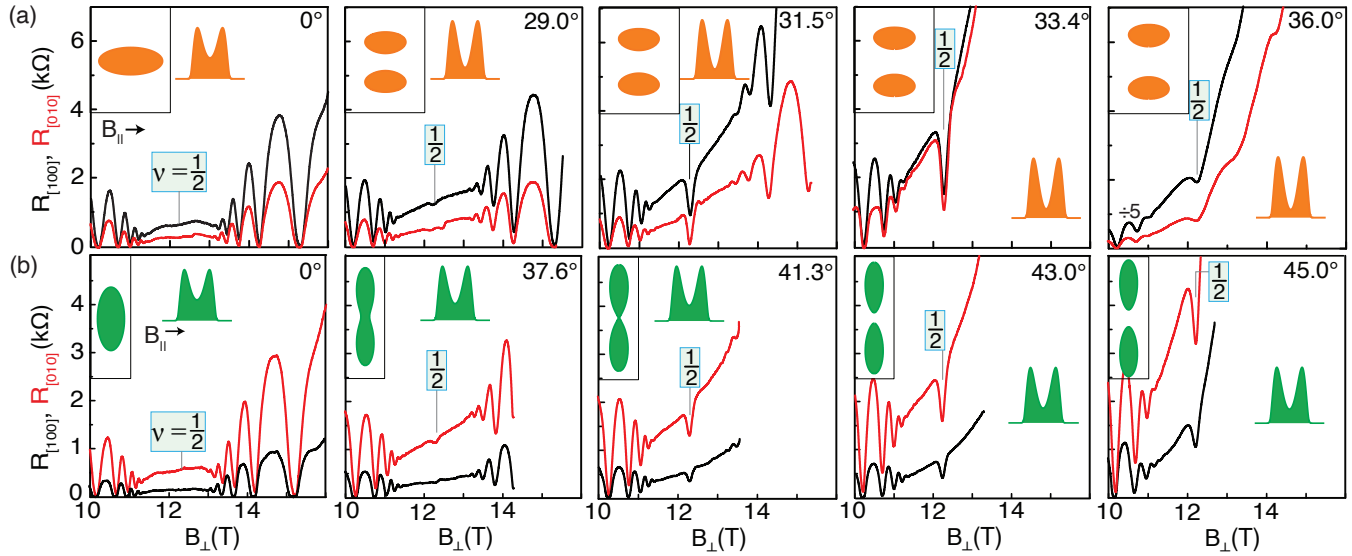


FIG. S6. Tilt-evolution of magnetoresistance data near $\nu = 1/2$ for different valley occupancies, all taken at $T \simeq 0.03$ K. The direction of $B_{||}$ is along [100], i.e., along $R_{[100]}$. (a) and (b) contain data for cases when the electrons occupy only X ($\varepsilon = -1.7 \times 10^{-4}$) or only Y ($\varepsilon = 1.7 \times 10^{-4}$) valley, respectively. In both (a) and (b), with increasing θ, the 2DES at $\nu = 1/2$ undergoes transitions from a compressible phase to an incompressible FQHS, and then finally to an insulating phase. However, the transitions happen at relatively smaller θ for case (a) where the electrons occupy only the X valley. Insets in each panel show the calculated electron charge distribution and Fermi seas for the corresponding $B_{||}$ that is experienced by the electrons at $\nu = 1/2$.

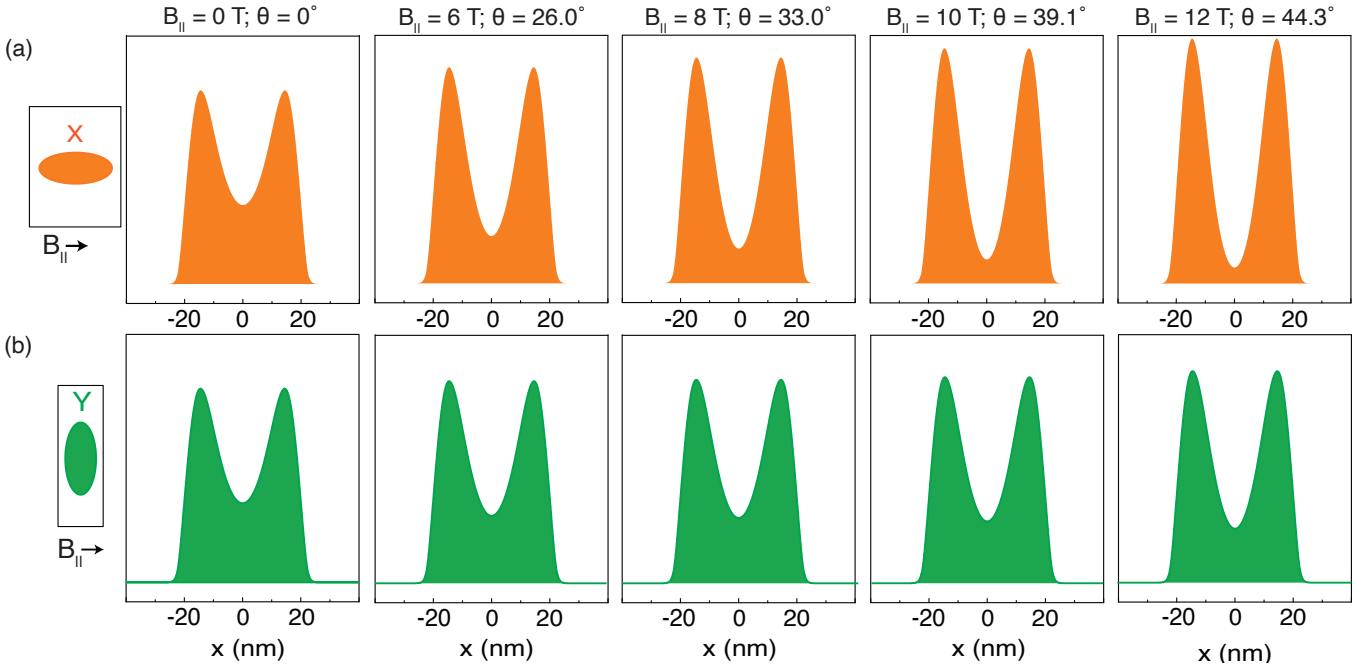


FIG. S7. Evolution of electron charge distribution as a function of $B_{||}$ for different valley occupancies. Plotted are the calculated electron charge distribution for $B_\perp = 0$ and $B_{||} = 0$ T, 6 T, 8T, 10 T, and 12 T, applied along [100], when the electrons occupy only (a) X and (b) Y valley. The plots clearly show that, at a given $B_{||}$, the 2DES becomes more bilayer like when it occupies the X valley.

valley occupancies are the same. However, the charge distribution and interlayer tunneling for the two valley occupancies exhibit clear differences when a finite $B_{||}$ is applied along [100]. The interlayer tunneling is smaller for the X-valley occupancy at a given $B_{||}$, which is the likely cause for the difference in $B_{||}$ required to observe

a strong FQHS at $\nu = 1/2$ for X vs. Y valley electrons.

Our numerical calculations also provide a plausible reason for the difference in the energy gap of $\nu = 1/2$ FQHS for X vs. Y valley electrons; see Fig. 4 of the main text. As seen in the insets of Fig. S6, the electron Fermi sea experiences different distortions resulting from $B_{||}$ applied along [100], for two different valleys occupancies. From our self-consistent calculations, we find mass anisotropy ratios $m_{[100]}/m_{[010]} \simeq 3.4$ for X-valley electrons at $B_{||} = 7.7$ T and $m_{[010]}/m_{[100]} \simeq 8.2$ for Y-valley electrons at $B_{||} = 11.7$ T where the 1/2 FQHS is strong. The much larger mass anisotropy for the Y-valley electrons might explain the smaller energy gap for the $\nu = 1/2$ FQHS. Larger mass anisotropy is generally expected to weaken the FQHSs [11], although the energy gaps could be quite robust and very large anisotropies would be needed to reduce the gaps significantly [12, 13]. Besides Fermi sea anisotropy, it is also likely that the different energy gaps measured in Figs. 4(c,d) result from the different electron charge distributions and tunneling for the different valley populations and different $B_{||}$ (Fig. S6 insets).

Lastly, it is worthwhile emphasizing that our calculations assume $B_\perp = 0$ and do not take electron correlations into account. Therefore, they cannot fully capture the connectivity and interlayer tunneling in the *composite fermion* Fermi sea at and near $\nu = 1/2$. As shown in Ref. [7], at large $B_{||}$, the *electron* Fermi sea in a quasi-2DES indeed splits and shows a bilayer behavior when a large $B_{||}$ is applied. In the presence of a large $B_\perp$, however, the measured Fermi sea for the *composite fermions* near $\nu = 1/2$ remains connected at large $B_{||}$ and exhibits only moderate anisotropy [14]. This is true whether the ground state at $\nu = 1/2$ is compressible [14], or is an incompressible FQHS [15]. In the case of an incompressible, composite fermion, ground state at $\nu = 1/2$, the experimental finding of the connectivity of the composite fermion Fermi sea has been corroborated qualitatively by numerical, many-body calculations [16]. Therefore, more accurate, many-body calculations are required to fully understand the $B_{||}$-evolution of the ground state at $\nu = 1/2$ presented in our paper.

V. EVOLUTION OF MAGNETOTRANSPORT WITH STRAIN

In Fig. S8 we show the magnetoresistance data, at $\theta \simeq 0^o$ and $T \simeq 0.03$ K, taken for different valley occupancies. The high magnetic field data shown in Fig. S6 demonstrate resistance anisotropy depending on the valley occupancy. Note that in all traces there is no FQHS at $\nu = 1/2$; instead, the ground state is a compressible, composite fermion Fermi sea. The traces also reveal the presence of higher-order FQHSs, up to $\nu = 7/15$ and 7/13, attesting to the excellent sample quality.

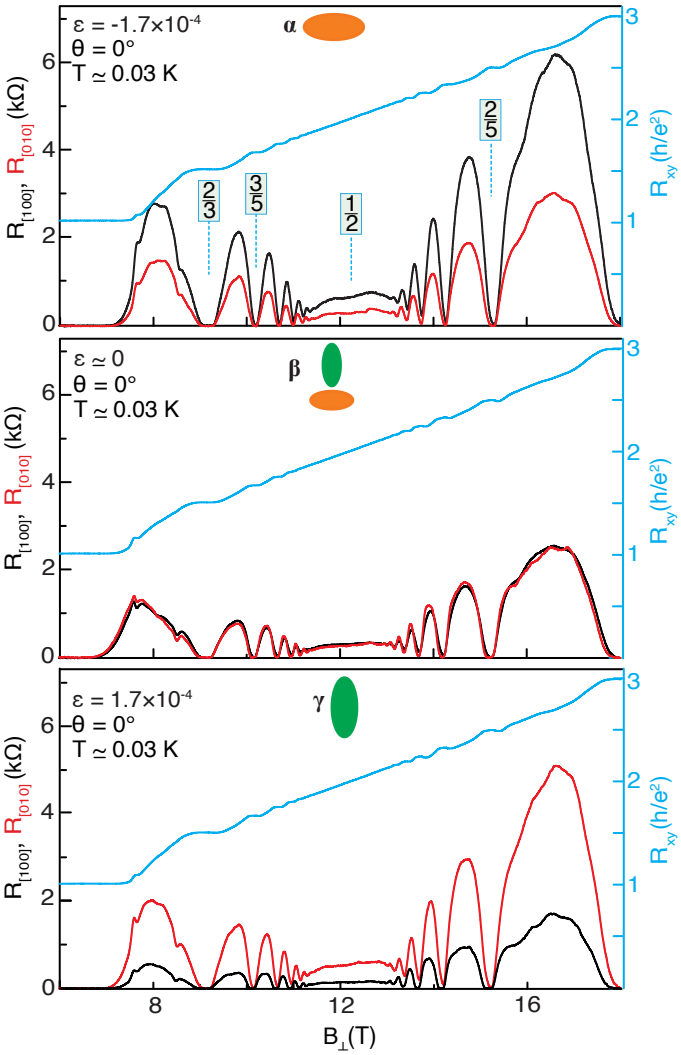


FIG. S8. Magnetotransport traces for different valley occupancy showing numerous odd-denominator FQHSs. Plotted are the $R_{[100]}$ (black), $R_{[010]}$ (red), and R_{xy} (blue) traces, taken at $\theta = 0^o$ and $T \simeq 0.03$ K, at three strain values as indicated. Note that the total density of the 2DES remains fixed as the electrons are transferred between the two valleys.

VI. VALLEY DEPENDENCE OF THE TILT EVOLUTION

In this section, we look more closely at the effect of the valley occupancy on the tilt evolution of the ground state $\nu = 1/2$. In Fig. S9 we show magnetoresistance data for different values of ε, taken at four different tilt angles. We start with $\theta = 0^o$ [Fig. S9(a)] where the ground state at $\nu = 1/2$ is a composite fermion Fermi sea for all strain values. As we tune the valley occupancy via applying the strain, the ground state at $\nu = 1/2$ remains the same. At $\theta = 32.7^o$ [Fig. S9(b)], there is a well-developed FQHS at $\nu = 1/2$ when $\varepsilon = -1.7 \times 10^{-4}$ and all the electrons are in the X valley. As we tune the

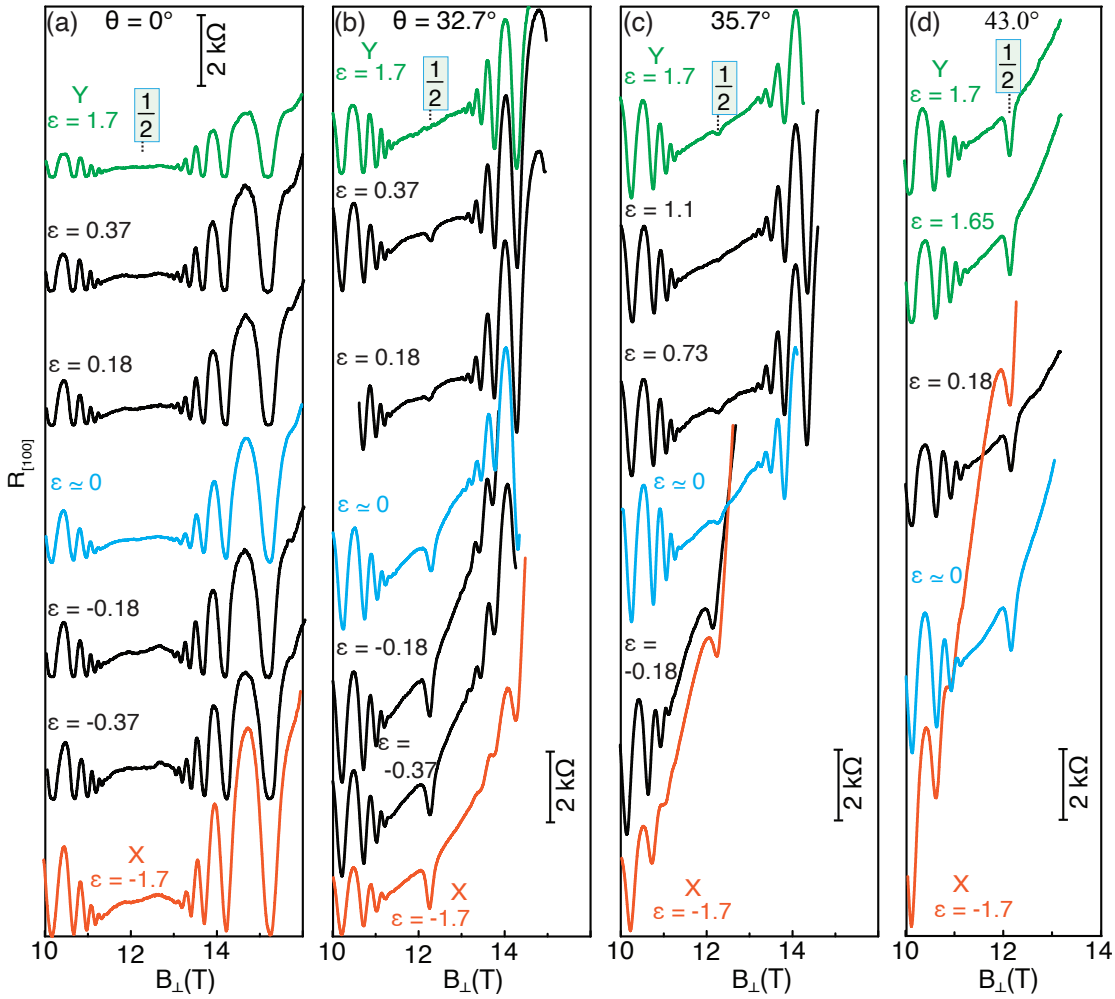


FIG. S9. Strain-dependent evolution of the magnetoresistance in the extreme quantum limit. Plotted are the magnetoresistance traces for four tilt angles, (a) $\theta = 0^o$, (b) $\theta = 32.7^o$, (c) 35.7^o, and (d) 43.0^o, all taken at $T \simeq 0.03$ K. The traces are vertically offset for clarity, and their corresponding strain value ε (in units of 10^{-4}) is denoted. The panels summarize the effect of the valley tuning on the $\nu = 1/2$ FQHS.

occupancy and transfer electrons to the Y valley, the $\nu = 1/2$ FQHS becomes progressively weak. Finally, when we place all the electrons in the Y valley, the $\nu = 1/2$ FQHS disappears.

At a slightly larger tilt angle, $\theta = 35.7^o$ [Fig. S9(c)], the $\nu = 1/2$ FQHS is on the verge of being engulfed by an insulating phase when the electrons are in the X valley ($\varepsilon = -1.7 \times 10^{-4}$). At $\nu < 1/2$, the 2DES becomes insulating. However, when we shift the population towards the Y valley, a weak $\nu = 1/2$ FQHS emerges and the insulating phase disappears.

Finally, at $\theta = 43.0^o$ [Fig. S9(d)], when the electrons are in the X valley, insulating phases take over on the two flanks of $\nu = 1/2$. As we move electrons from X to Y valley, the $\nu = 1/2$ FQHS becomes more pronounced and the insulating phase on the low-field flank of $\nu = 1/2$ FQHS goes away.

These measurements clearly show the effectiveness of strain, as well as tilt angle, as tuning parameters to control the ground state at and near $\nu = 1/2$.

[1] T. S. Lay, J. J. Heremans, Y. W. Suen, M. B. Santos, K. Hirakawa, and M. Shayegan, High-quality two-dimensional electron system confined in an AlAs quantum well, Appl. Phys. Lett. **62**, 3120 (1993).

[2] E. P. De Poortere, Y. P. Shkolnikov, E. Tutuc, S. J. Papadakis, and M. Shayegan, Enhanced electron mobility and high order fractional quantum Hall states in AlAs quantum wells, Appl. Phys. Lett. **80**, 1583 (2002).

[3] M. Shayegan, E. P. De Poortere, O. Gunawan, Y. P. Shkolnikov, E. Tutuc, and K. Vakili, Two-dimensional electrons occupying multiple valleys in AlAs, Phys. Stat. Sol. (b) **243**, 3629 (2006).

[4] Y. J. Chung, K. A. Villegas Rosales, H. Deng, K. W. Baldwin, K. W. West, M. Shayegan, and L. N. Pfeiffer,

Multivalley two-dimensional electron system in an AlAs quantum well with mobility exceeding 2×10^6 cm^2/Vs, Phys. Rev. Materials **2**, 071001(R) (2018).

[5] M. Shayegan, K. Karrai, Y. P. Shkolnikov, K. Vakili, E. P. De Poortere, and S. Manus, Low-temperature, in situ tunable, uniaxial stress measurements in semiconductors using a piezoelectric actuator, Appl. Phys. Lett. **83**, 5235 (2003).

[6] T. Gokmen, M. Padmanabhan, O. Gunawan, Y. P. Shkolnikov, K. Vakili, E. P. De Poortere, and M. Shayegan, Parallel magnetic-field tuning of valley splitting in AlAs two-dimensional electrons, Phys. Rev. B **78**, 233306 (2008).

[7] M. A. Mueed, D. Kamburov, M. Shayegan, L. N. Pfeiffer, K. W. West, K. W. Baldwin, and R. Winkler, Splitting of the Fermi Contour of Quasi-2D Electrons in Parallel Magnetic Fields, Phys. Rev. Lett. **114**, 236404 (2015).

[8] W. Zhu, Zhao Liu, F. D. M. Haldane, and D. N. Sheng, Fractional quantum Hall bilayers at half filling: Tunneling-driven non-Abelian phase, Phys. Rev. B 94, 245147 (2016).

[9] W. N. Faugno, Ajit C. Balram, Maissam Barkeshli, and J. K. Jain, Prediction of a Non-Abelian Fractional Quantum Hall State with f -Wave Pairing of Composite Fermions in Wide Quantum Wells, Phys. Rev. Lett. **123**, 016802 (2019).

[10] T. Zhao, W. N. Faugno, S. Pu, A. C. Balram, and J. K. Jain, Origin of the $\nu = 1/2$ fractional quantum Hall effect in wide quantum wells, Phys. Rev. B **103**, 155306 (2021).

[11] H. Wang, R. Narayanan, X. Wan, and F. Zhang, Fractional quantum Hall states in two-dimensional electron systems with anisotropic interactions, Phys. Rev. B **86**, 035122 (2012).

[12] I. Jo, K. A. Villegas Rosales, M. A. Mueed, L. N. Pfeiffer, K. W. West, K. W. Baldwin, R. Winkler, M. Padmanabhan, and M. Shayegan, Transference of Fermi contour anisotropy to composite fermions, Phys. Rev. Lett. **119**, 016402 (2017).

[13] Ajit C. Balram and J. K. Jain, Exact results for model wave functions of anisotropic composite fermions in the fractional quantum Hall effect, Phys. Rev. B **93**, 075121 (2016).

[14] D. Kamburov, M. A. Mueed, M. Shayegan, L. N. Pfeiffer, K. W. West, K. W. Baldwin, J. J. D. Lee, and R. Winkler, Fermi contour anisotropy of GaAs electron-flux composite fermions in parallel magnetic fields, Phys. Rev. B **89**, 085304 (2014).

[15] M. A. Mueed, D. Kamburov, S. Hasdemir, M. Shayegan, L. N. Pfeiffer, K. W. West, and K. W. Baldwin, Geometric Resonance of Composite Fermions Near the $\nu = 1/2$ Fractional Quantum Hall State, Phys. Rev. Lett. **114**, 236406 (2015).

[16] M. Ippoliti, Scott D. Geraedts, and R. N. Bhatt, Connection between Fermi contours of zero-field electrons and $\nu = 1/2$ composite fermions in two-dimensional systems Phys. Rev. B **96**, 045145 (2017).